Fluid dynamics characterisation of a rotating bioreactor for tissue engineering

Agnès Drochon[a*], Romane Lesieur[b, c, d] , Marlène Durand[b, c, d]

[a] CNRS, University of Bordeaux, Arts et Metiers Institute of Technology, Bordeaux INP, INRAE, I2M Bordeaux, F-33400 Talence, France

[b] Univ. Bordeaux, CIC 1401, INSERM, Institut Bergonié, F-33000, Bordeaux, France

[c] CHU Bordeaux, CIC 1401, F-33000, Bordeaux, France

[d] Univ. Bordeaux, BIOTIS UMR 1026, INSERM, F-33000, Bordeaux, France

*Corresponding author: agnes.drochon@u-bordeaux.fr

ABSTRACT : (*155 words)*

Biological scaffolds composed of extracellular matrix (ECM) derived from decellularised tissue are increasingly used in regenerative medicine. In this project, a flow perfusion bioreactor (the rotary cell culture system (RCCS), commercially available from Synthecon (Houston, TX)) is used in order to obtain some esophageal extracellular matrix. A theoretical mechanical characterisation of this experimental set-up is provided. Due to the combination of rotation and perfusion, some spiral Poiseuille flow is created inside the tubular esophagus. In a transverse section, a particle (or cell) experiences simultaneously gravitational, Archimedes, centrifugal, Coriolis, and drag forces. In a frame of reference rotating with angular velocity ω, the particle follows a periodic nearly circular path in the clockwise direction, associated with a very slow centrifugal drift towards the esophagus wall. It appears that moderate perfusion rate and rotation speed ($\omega < 20$ rpm and $Q < 30$ ml/min) are appropriate experimental conditions for esophagus tissue engineering using the RCCS Synthecon bioreactor.

Keywords : rotating bioreactor; spiral Poiseuille flow; esophageal substitute; tissue engineering

Paper word count (total) : 7300 words.

1. Introduction

The concepts of tissue engineering and regenerative medicine are used to develop therapeutic alternatives in order to provide viable solutions for patients waiting for a transplant of a failing organ in terminal phase [1]. Increasingly used in regenerative medicine, biological scaffolds composed of an extracellular matrix (ECM), derived from decellularised tissues, are able to satisfy some clinical needs [2]. However, the decellularisation process must not compromise the integrity of the native organ's overall three-dimensional architecture, structural components and biomechanical properties. Different methods have been developed to this aim [1].

Esophageal tissue engineering is a promising approach to the treatment of esophageal pathologies such as esophageal atresia, which affects one newborn for every 3,500 births [3], esophageal cancer, which is the eight most common cancer in the world [4], accidental or intentional burns, and perforations. Currently, the restoration of digestive continuity after esophagectomy is achieved through the interposition of a segment of the colon or by the tubulation of the stomach (Lewis Santy intervention); however there are many post-operative complications such as anastomotic leaks, infections, etc. [5]. There has been interest shown in the development of a tissue-engineered esophageal substitute, constituted of an acellular matrix and seeded cells, for the treatment of esophageal pathologies. It is necessary to develop optimal decellularisation techniques in order to obtain a clinical grade esophageal ECM for full thickness esophageal replacement. Previous studies have developed an acellular esophageal substitute from skin, urinary bladder, intestinal submucosa from various animal and human models; however, the use of porcine esophagus has been shown to be the most adapted tissue engineering support for a full thickness esophageal replacement. The use of decellularisation solutions in contact with native esophageal tissue ensures the removal of

cellular content and DNA. In recent years, different decellularisation solutions have been explored such as sodium dodecyl sulfate, sodium deoxycholate, Triton X-100, and Chaps [6]. The most effective decellularisation procedure for engineering an acellular scaffold from a porcine esophageal sample was found to be the use of sodium deoxycholate for cell lysis coupled with DNAse I for the removal of DNA [7]. The action of these chemical and enzymatic solutions can be amplified by a mechanical action provided by immersion under constant agitation, or by using the esophageal lumen as a perfusion way [8], [9]. In this study, the decellularisation of a porcine esophagus sample is made possible by the perfusion of sodium deoxycholate solutions coupled to DNase I, in order to provide biological scaffolds able to be recellularised by human stem cells [9]. The functionalisation of an esophageal substitute by a recellularisation method is a significant challenge in tissue regeneration after transplantation of a tissue engineered organ [1]. It is possible to recellularise esophageal decellularised matrices (DM) with several cell types: autologous or allogeneic, differentiated or non-differentiated. The use of cell sheets [9] allows the recellularisation of DM under static conditions, whereas recellularisation with suspended cells requires a dynamic environment to overcome the sedimentation phenomenon [6]. For this purpose, a flow perfusion bioreactor is used: the rotary cell culture system (RCCS), commercially available from Synthecon (Houston, TX) [10]. This device allows liquid flow within the tubular esophagus as well as a mechanical rotation in and around the tissue in two successive closed chambers. The flow of this liquid is thus controlled according to a perfusion flow rate and a rotation of the chamber. Thanks to this dynamic environment in the bioreactor the distribution of the seeded cells in the DM is performed in a homogenous way [6]. The aim of this paper is to provide a theoretical mechanical characterization of this experimental set-up in order to determine: i) the velocity fields, pressures, shear stresses in the fluid without suspended cells, ii) the forces that act on a suspended cell and determine its motion.

Although several papers [11-15] mention the basic principle of rotating wall bioreactors the literature survey did not allow us to find a convenient detailed mechanical and mathematical

analysis of the combined rotation and perfusion movement in such devices. Pollack et al. [16] provided the equations of motion for microcarriers in a rotating bioreactor. They validated their analysis with some experimental and numerical results. However, they used a High Aspect Ratio Vessel (HARV). This type of bioreactor has a large radius to depth ratio, it looks like a disk and not like a cylinder. Their analysis was 2D (no longitudinal motion). The HARV was also used by Mazzoleni et al. [17] as an in-vitro model of osteocytes' differentiation and bone matrix formation, and by Ferrarini et al. [18] as a tool to study 3-D tumor (myeloma) models. Varley et al. [19] used a more common type of bioreactor, named RWV (Rotating Wall Vessel), to improve osteoblasts proliferation in floating scaffolds. They proposed a dual-axis rotating system with rotation speeds of each axis in the range 5- 35 rpm. They performed some numerical calculations but they did not provide information about their numerical procedure. They considered the case where the bioreactor chamber is not 100% filled with culture medium. Consequently, they had to take into account a fluid /air interface with its specific boundary condition. Liu et al. [20] published an analysis on forces and movement of cultivated particles in a rotating wall vessel bioreactor. They considered the case where the rotating speeds (in the range 10 r.p.m. to 65 r.p.m.) of the inner and outer cylinders are not the same. No longitudinal flow exists in their study and the sizes of the suspended particles are in the range 100 μm to 1 mm. Their equations and mathematical solution seem very questionable. Some longitudinal flow is considered in [21] but the bioreactor used by these authors is very different from the one we use. Their bioreactor is composed of two concentric cylinders that can be independently rotated (15-35 r.p.m.). The fluid is tangentially perfused between the inner and outer cylinders. Since the inner cylinder wall is porous, the fluid is collected in the inner cylinder and goes back to the external flow loop. Their perfusion rate is typically 10 ml/min. They provide a numerical solution for the flow fields and shear stresses but do not study the motion of suspended particles.

In 2014, Grimm et al. [22] published an extensive review of the existing devices that simulate microgravity and can be used for various tissue engineering applications. A literature

synthesis on bioreactors and their utilisation in bone tissue engineering can also be found in [23]. Some studies mention the use of a RCCS bioreactor and provide details about their experimental procedures, but they do not give any mechanical analysis; for example, the experimental conditions are: no longitudinal flow, low rotational speed (10 r.p.m.) in the study of Morabito et al. [24] and no longitudinal flow, rotational speeds in the range 12 to 22 r.p.m. in the study of Lei et al. [25].

Other experimental studies demonstrate that the concept of rotating wall bioreactor associated with longitudinal perfusion is pertinent for decellularisation and recellularisation of tissue engineered tubular constructs. A double-chamber tracheal bioreactor is described in [26]. More recently, this device has been re-designed by Lee et al. [27] to improve the perfusion cell seeding protocol in order to re-epithelialise de-epithelialised tracheal scaffolds. A tracheal rotation along its longitudinal axis is allowed from 0 to 30 rpm, with flow rates range from 1.5 to 12 ml/min. This favours circulation and mixing of micronutrients and provides control of the cell deposition patterns on the scaffold. Nayakawde et al. [7] also perform recellularisation of acellular esophagus matrix in a perfusion-rotation bioreactor (Harvard Apparatus) with very slow flow rate (3 ml/min) and rotation (0.5 r.p.m.). Urbani et al. [28] use an Applikon bioreactor connected to a reservoir medium to create dynamic cell culture conditions on their esophagus scaffolds. No rotation is possible with this device and the medium flow rate is 5 ml/min. The flow loop is ensured by peristaltic pumps in [7, 27, 28] and by a home-made motion unit in [26].

2. Materials and methods

2.1.Description of the perfusion bioreactor and closed flow loop

A schematic representation of the RCCMax-dual esophagus bioreactor and of the flow bench is reported in **Figure 1**. The bioreactor consists of two successive cylinder chambers that rotate horizontally at the same constant angular speed. Some direct motor drive is used to

rotate the cylinders. In each chamber there are scaffold holders on which a tubular scaffold can be mounted and tied with a non-absorbable 2/0 USP suture. The scaffold thus rotates at the same angular velocity as the chamber wall. The chambers are connected to a media reservoir bottle, an oxygenator and a 4-rollers peristaltic pump (Watson Marlow 314D). One r.p.m. on the peristaltic pump provides a 0.5 ml/min flow rate through the tubing. Silicon tubing has a wall tube thickness 1.6 mm and internal diameter 1.6 mm. The oxygenator uses silicone membrane diffusion of gases. The reservoir is open to atmospheric pressure. The circulating medium contains Sodium Azide, Sodium Deoxycholate and DNaseI.

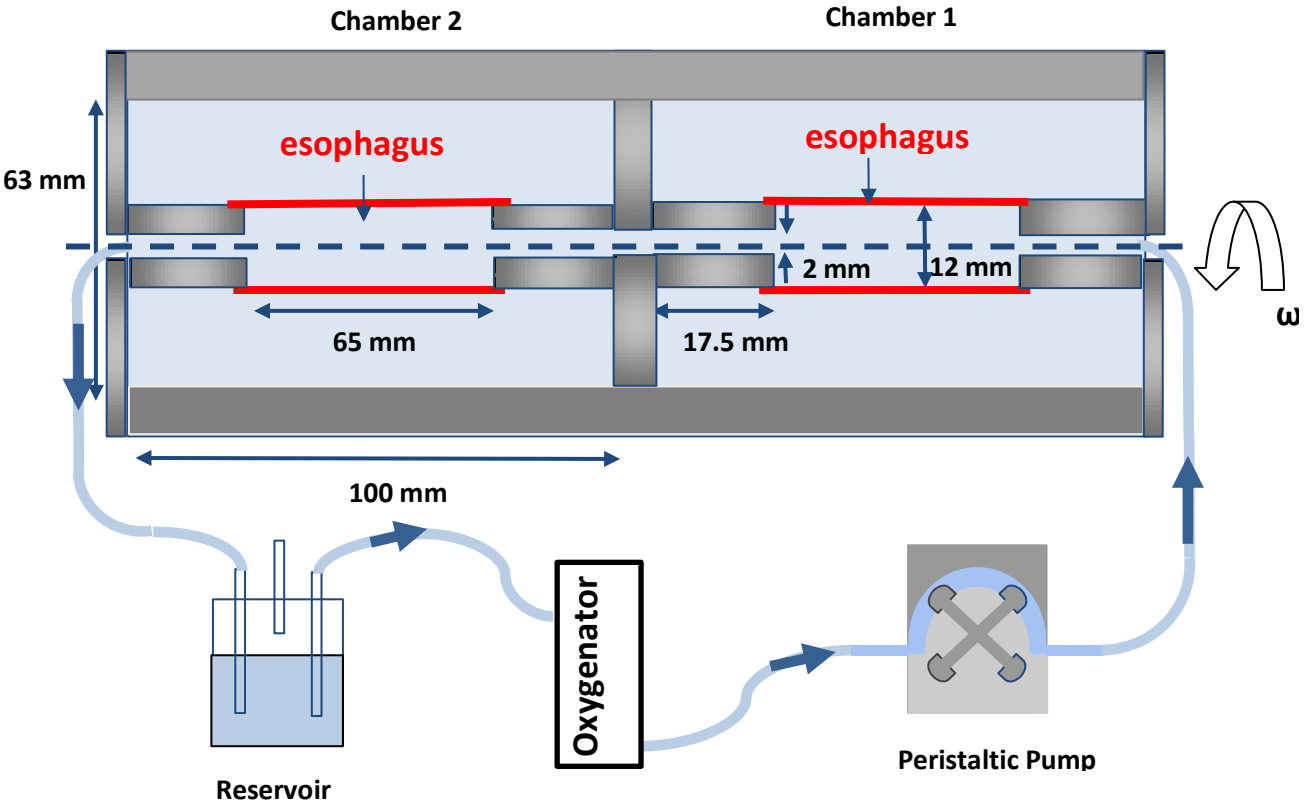

Figure 1 - Schematic representation of the experimental set-up.

2.2. Analytical approach

2.2.1. Fluid motion

The fluid medium used for the decellularisation experiments is considered as newtonian with a viscosity η_f = 1 mPas and a density ρ_f = 1015kg/m^3. For the moment the esophagus wall is

assumed non-deformable and non-porous and its thickness (a few millimeters) is not taken into account. R_1 denotes the esophagus radius (R_1 = 6 mm) and R_2 the chamber radius (R_2 = 31.5 mm). Both cylinders (esophagus and chamber) are supposed "infinitely" long with an axial symmetry.

In each chamber of the bioreactor two distinct parts will be considered: **Part A** will refer to the perfusion inside the esophagus and **Part B** will refer to the medium enclosed between the esophagus and the chamber wall. The scaffold is attached to some part of the chamber; consequently the esophagus wall rotates at the same angular velocity as the chamber wall.

In **Part B** there is no fluid circulation (no longitudinal fluid velocity). The fluid rotates as a rigid body with an angular velocity ω throughout the domain (Couette flow). In classical cylindrical coordinates (O, r, θ, z) this would yield: no radial velocity and an azimuthal velocity U_θ equal to ω r, r being the radial coordinate ($R_1 < r < R_2$). In this environment, shear stresses are null.

In **Part A** for a given value of the pump flow rate (Q) quantities of interest do not depend on time. The flow is driven by the combination of two factors: a constant axial pressure gradient (along Oz) and the rotation of the dual chamber. Velocity continuity prevails at the wall, due to the no-slip boundary conditions. This results in an exact superposition of an axial parabolic velocity profile U_z and an azimuthal solid-body rotation U_θ depending only on the radial coordinate r as:

$$U_z(r) = 2\,U_{mean}\,(1-\frac{r^2}{R_1^2})\,, \quad \text{and} \quad U_\theta(r) = \omega\, r \tag{1}$$

where U_{mean} is the mean axial velocity associated with the axial pressure gradient ($-\frac{\partial P^*}{\partial z}$) according to:

$$U_{mean} = \frac{Q}{\pi R_1^2} = \frac{\left(-\frac{\partial P^*}{\partial z}\right) R_1^2}{8\eta_f} \tag{2}$$

This type of flow is known as the rotating Hagen-Poiseuille flow or spiral-Poiseuille flow [29]. It is characterized by two non-dimensional control parameters: the streamwise Reynolds number:

$$R_{ez} = \frac{\rho_f \ U_{mean} \ (2 R_1)}{\eta_f} \quad (3)$$

and the azimuthal (or rotational) Reynolds number:

$$R_{e\omega} = \frac{\rho_f (\omega R_1)(2 R_1)}{\eta_f} \quad (4)$$

In such a flow, tangential shear stresses in the azimuthal direction are null since:

$$\tau_{r\theta} = \eta_f r \frac{\partial}{\partial r}\left(\frac{U_\theta}{r}\right) \quad (5),$$

and tangential shear stresses in the axial direction may be calculated as:

$$\tau_{rz} = \eta_f \frac{\partial U_z}{\partial r} = -\frac{r}{2}\left(-\frac{\partial P^*}{\partial z}\right) \quad (6).$$

They are maximal at the wall of the esophagus (r = R_1).

It is important to mention that both in **Part A** and **B**, the radial projection of Navier-Stokes equations can be simplified as:

$$\frac{\partial P^*}{\partial r} = \rho_f \frac{U_\theta^2}{r} = \rho_f \frac{\omega^2 r^2}{r} = \rho_f \omega^2 r \quad (7),$$

thus demonstrating that a positive radial pressure gradient exists in each domain.

2.2.2. Suspended particle motion

In order to be able to describe the motion of a particle relative to the rotating fluid a rotating frame (O, x, y, z) is considered (**Figure 2**). Conversely (O, X, Y, Z) is a ground-based frame (fixed). Since the esophagus cylinder and the chamber cylinder are concentric, the (OZ) and (Oz) axis are the same. Unit vectors associated with (OXY) are denoted $\mathbf{e_X}$ and $\mathbf{e_Y}$, and unit vectors associated with (Oxy) are denoted $\mathbf{e_x}$ and $\mathbf{e_y}$. The (Oz) and (OZ) unit vectors are denoted $\mathbf{e_z}$, so that the frames are direct. The frame (O, x, y, z) rotates counter-clockwise about the (Oz) axis with a constant angular velocity ω. The rotating vector is thus: $\mathbf{\Omega} = \omega \mathbf{e_z}$.

We consider a non-deformable spherical particle with radius a and density ρ_p (slightly higher than the fluid density ρ_f). The mass of the particle is thus:

$m_P = \rho_P V_P$, where V_p is the particle volume ($V_P = \frac{4}{3}\pi a^3$) .

Since the particle is positively buoyant, it experiences sedimentation while the chamber and the fluid are rotating.

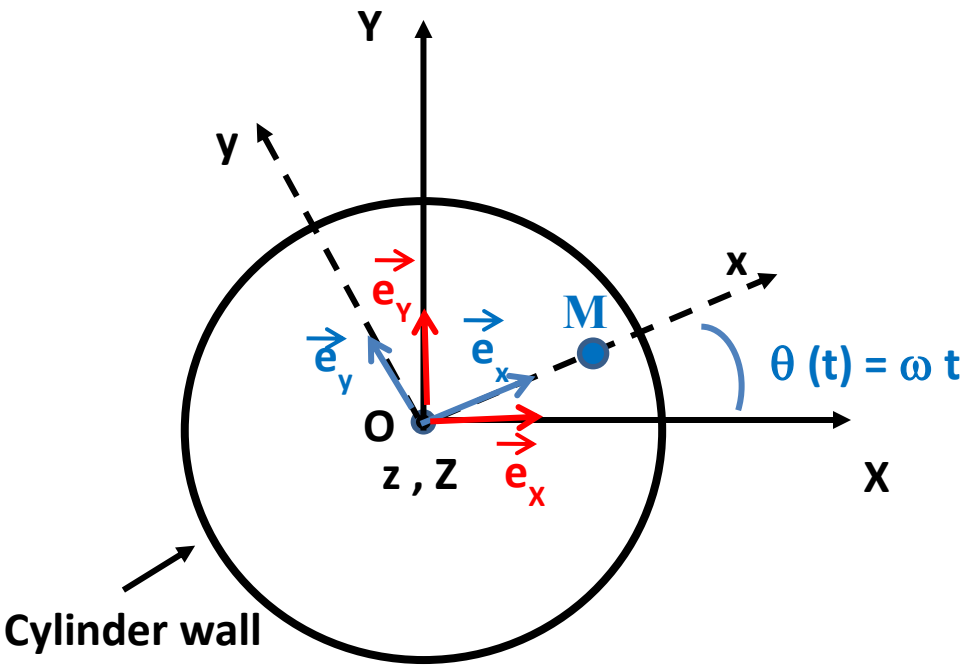

Figure 2 – Ground-based and rotating cylindrical frames: definition of the notations. The gravitational acceleration **g** is perpendicular to the rotation axis (Oz); it is directed down the (OY) axis.

The particle position (**OM**) , velocity (**v**) and acceleration (**a**) in the rotating frame are respectively :

$\boldsymbol{OM} = \begin{vmatrix} x \\ y \\ z \end{vmatrix}$, $\mathbf{v} = \begin{vmatrix} \dot{x} \\ \dot{y} \\ \dot{z} \end{vmatrix}$, $\boldsymbol{a} = \begin{vmatrix} \ddot{x} \\ \ddot{y} \\ \ddot{z} \end{vmatrix}$, where the dot denotes time derivative

of a quantity. Accordingly the entrainment velocity is obtained as:

$$\boldsymbol{\Omega} \wedge \boldsymbol{OM} = \begin{vmatrix} 0 \\ 0 \\ \omega \end{vmatrix} \wedge \begin{vmatrix} x \\ y \\ z \end{vmatrix} = \begin{vmatrix} -\omega y \\ \omega x \\ 0 \end{vmatrix} \quad (8)$$

The entrainment acceleration is :

$$\boldsymbol{\Omega} \wedge (\boldsymbol{\Omega} \wedge \boldsymbol{OM}) = \begin{vmatrix} 0 \\ 0 \\ \omega \end{vmatrix} \wedge \begin{vmatrix} -\omega y \\ \omega x \\ 0 \end{vmatrix} = \begin{vmatrix} -\omega^2 x \\ -\omega^2 y \\ 0 \end{vmatrix} \quad (9),$$

And the Coriolis acceleration is:

$$\mathbf{2}\,\boldsymbol{\Omega} \wedge \boldsymbol{v} = \begin{vmatrix} \mathbf{0} \\ \mathbf{0} \\ 2\,\omega \end{vmatrix} \wedge \begin{vmatrix} \dot{x} \\ \dot{y} \\ \dot{z} \end{vmatrix} = \begin{vmatrix} -2\,\omega\dot{y} \\ 2\,\omega\,\dot{x} \\ 0 \end{vmatrix} \quad (10)$$

In **Part B** the particle experiences simultaneously gravitational, Archimedes, centrifugal, Coriolis, and drag forces.

Introducing a buoyancy corrected mass, $m_b = (\rho_p - \rho_f)\, V_p$, the buoyancy corrected weight of the particle is: m_b **g**, where we have to consider the projection of the gravitational acceleration **g** in the rotating frame:

$$\boldsymbol{g} = \begin{vmatrix} -g\sin(\omega t) \\ -g\cos(\omega t) \\ 0 \end{vmatrix} \quad (11).$$

Since the particle is small and the velocities are moderate, an appropriate estimation of the viscous drag may be obtained using Stokes approximation:

D = - k **v**, where the coefficient k is given by : $6\pi\,\eta_f\,a$ (12).

Since the fluid is in solid body rotation the pressure gradient acting on ($\rho_f V_p$) opposes the the centripetal force on ($\rho_p V_p$) and the resulting force will be written as:

$$\begin{vmatrix} -m_b\,\omega^2 x \\ -m_b\,\omega^2\,y \\ 0 \end{vmatrix} \quad (13)$$

Gathering all, in **Part B**, the motion of the particle in the rotating frame is governed by the following differential equations:

$$m_P\,\ddot{x} = -k\dot{x} + m_b\omega^2 x + 2m_p\omega\dot{y} - m_b\,g\,sin\,(\omega t) \quad (14)$$

$$m_P\,\ddot{y} = -k\dot{y} + m_b\omega^2 y - 2m_p\omega\dot{x} - m_b\,g\,cos\,(\omega t) \quad (15)$$

Equations (14-15) indicate that particle motion may be affected by: density difference between fluid and particle vessel rotation rate, fluid viscosity and particle radius.

In **Part A**, due to the fluid perfusion a longitudinal motion of the particle exists. The equation of motion for the relative particle displacement is:

$$m_P\,\ddot{z} = -k\dot{z} \qquad (16)$$

Additionally the Poiseuille flow shear rate (radial variation of the longitudinal velocity) can induce a torque on the particle associated with a lift force and a radial migration [30]. This shear rate can be derived from Equ.(1) and (2) as follows:

$$G = \frac{\partial U_z}{\partial r} = -\frac{4\,Q\,r}{\pi R_1^4} \qquad (17).$$

A Reynolds number based upon the particle radius and the averaged velocity gradient, G_{mean}, can be defined as:

$$R_{eG} = \frac{\rho_f \;\; G_{mean}\; a^2}{\eta_f} \qquad (18)\,,$$

where $G_{mean} = -\frac{2\,Q}{\pi R_1^3}$.

3. Results

3.1.Reynolds numbers, entry lengths and pressure losses in the bioreactor

The effects of changes in operating conditions including rotation rates and fluid perfusion rates, are investigated. The chosen values are in agreement with the literature survey that is summarised in the "Introduction" Section. Slightly upper-range values are also selected in order to determine whether they would be acceptable or not for this type of tissue engineering applications.

The mean axial velocity in the esophagus, U_{mean} , is obtained from Equ. (2) with a diameter of the lumen $2R_1$ = 12 mm. The mean axial velocity in the lumen of the scaffold holder (diameter d = 2 mm) is denoted u_{mean} , and calculated as : $u_{mean} = 4Q/\pi d^2$. The streamwise Reynolds number in the esophagus and the azimuthal Reynolds number are deduced from Equ. (3) and (4). An estimation of the flow entrance length is provided by the classical formula:

$$L_e \approx 0.05\; R_{ez}\,(2R_1) \qquad (19)$$

Viscous pressure losses due to the singularities at the entrance and at the exit of the chamber are respectively given by: $\Delta P_f^{ent.} = k_1 \frac{1}{2} \rho_f \, u_{mean}^2 \,, \; with \; k_1 = \left(1 - \left(\frac{d}{2\,R_1}\right)^2\right)^2$ (20)

and : $\Delta P_f^{exit.} = k_2 \frac{1}{2} \rho_f \, u_{mean}^2 \,, \; with \; k_2 = 0.5 \left(1 - \left(\frac{d}{2\,R_1}\right)^2\right)$ (21).

Since the flow rates are quite moderate, Equ. (22) provides a suitable evaluation of the pressure losses along the silicone tubing (l_{tube} = 0.5 m, d_{tube} = 1.6 mm):

$$\Delta P_f^{tube} = \frac{64}{R_e^{tube}} \frac{1}{2} \rho_f \, u_{tube}^2 \, \frac{l_{tube}}{d_{tube}}, \quad where \; R_e^{tube} = \frac{\rho_f \, u_{tube} \, d_{tube}}{\eta_f} \qquad (22).$$

The numerical values of all these quantities are gathered in **Table1**.

Flow rates and corresponding velocities

Q (ml/min)	12,50	25,00	50,00
U_{mean} (mm/s)	1,84	3,68	7,37
u_{mean} (mm/s)	66,3	133	265

Reynolds numbers and entry lengths in the esophagus

R_{ez} (Equ.(3))	22,43	44,87	89,74
L_e (Equ.(19)) (mm)	13,5	26,9	53,8
Le (% of the total esophagus length)	21	41	83

Pressure losses at the entrance and exit of the chamber

k_1 (Equ. (20))			0,9452
k_2 (Equ. (21))			0,4861
ΔP_f - Entrance (Pa) (Equ. (20))	2,11	8,44	33,74
ΔP_f – Exit (Pa) (Equ. (21))	1,085	4,34	17,35

Pressure losses along the tubing

u_{tube} (mm/s)	104	207	414
Reynolds-tubing (Equ. (22))	168,25	336,49	673,15
Pressure loss -tubing (Pa) (Equ. (22))	647,5	1 295	2 590,6

Azimuthal Reynolds number (Equ. (4))

ω (r.p.m.)	15	30
ωR_1 (mm/s)	9,42	18,85
Azimuthal Reynolds number	114,8	229,6

Table 1: Characteristic hydrodynamic data .

The data reported in Table 1 indicate that:

- the Reynolds numbers are sufficiently small for the flow to be considered laminar
- depending upon the operating conditions, the azimuthal velocity may be slightly higher than the longitudinal velocity
- pressure losses along the tubing are much more important than pressure losses at the entrance and at the exit of the chamber
- in order to get a fully developed flow in the esophagus, one has to keep the flow at low level. Otherwise the entrance length may represent a too important proportion of the total esophagus length.

3.2. Analytical approach

3.2.1. Streamlines in Spiral-Poiseuille flow (without particle)

Equations for the velocity field inside the esophagus (**Part A** of the flow domain) are given in Section 2.2.1 (Equations (1) and (2)). Reporting Equ.(2) in Equ.(1), the longitudinal velocity turns out to be:

$$U_z(r) = \frac{1}{4\,\eta_f}\left(-\frac{\partial P^*}{\partial z}\right)(R_1^2 - r^2) \qquad (23)$$

Fluid particles pathlines are determined by:

$$\begin{cases} dz = U_z(r)\,dt \\ d\theta = \omega\,dt \end{cases} \qquad (24).$$

Integrating and eliminating the variable t (time) one gets the streamline equation associated with the initial conditions z = 0 and θ = 0 at t = 0:

$$z = U_z(r)\,\frac{\theta}{\omega} \qquad (25).$$

Equation (25) describes an helix curve whose constant radius is r and whose pitch is :

$$h(r) = U_z(r)\,\frac{2\pi}{\omega} \qquad (26).$$

This result may be illustrated with specified values of r, Q and ω.

For example: r is chosen as R_1 / 2 (that is 3 mm), Q = 25 ml/min, and ω = 15 r.p.m.

With these numerical data,

351 U_{mean} = 3,68 mm/s; U_z (R_1/2) = 3 U_{mean} / 2 = 5,52 mm/s; h (R_1/2) = 22,1 mm .

352
353 *3.2.2. Motion of a spherical particle suspended in the fluid*
354
355 *Order of magnitude of Coriolis force on the particle.*
356
357 Let us suppose that a cell can be represented by a spherical particle with diameter 2a = 15
358 microns and density ρ_p = 1070 kg/m^3 (the cell volume V_p will thus be 1767 μm^3 and its mass
359 m_p = 1, 89 10^{-12} kg). We consider first the sedimentation equilibrium velocity, u_p, for such a
360 particle suspended in a non-rotating fluid. In these conditions the particle experiences drag
361 and Archimedes forces against gravity. All these forces are directed along (OY) (vertical).
362 The velocity u_p is given by the well-known Stokes formula:

363 $$u_p = \frac{2\,g\,(\rho_p - \rho_f)}{9}\,a^2\,\frac{1}{\eta_f} \qquad (27)$$

364 With our numerical data this yields: u_p = 6.74 μm/s, which is 3 orders of magnitude smaller
365 than the fluid velocities shown in Table 1.
366 Similarly a Reynolds number based on the particle diameter 2a and terminal velocity u_p can
367 be evaluated as: $$R_e^p = \frac{\rho_f\ 2a\ u_p}{\eta_f} \qquad (28)$$
368 Its value is: $R_e^p = 0.0001$ (five or six orders of magnitude smaller than the fluid
369 Reynolds).
370 Coming back to the rotating fluid and rotating frame (Oxyz) (Figure 2), the sedimentation
371 velocity u_p is the particle velocity relative to the rotating frame, and is thus involved in the
372 evaluation of Coriolis acceleration, for which the norm can be expressed as: 2 ω u_p.
373 For ω = 15 r.p.m., Coriolis acceleration scales as: 2,12 10^{-5} m/s^2. This has to be compared to
374 the centrifugal acceleration ω^{2}r. If the ω^{2}r term is evaluated at a radial distance r = 3 mm
375 (inside the esophagus) its value is 7,4 10^{-3} m/s^2; if it is evaluated at r = 2 cm (between the
376 esophagus and the chamber wall) , its value is 49,3 10^{-3} m/s^2 . It may thus be concluded that
377 the ratio of Coriolis acceleration to centrifugal acceleration is very small (of order 10^{-3}), and
378 that Coriolis force may probably be neglected in Equ. (14-15).

Importance of the lift effect on the particle in Poiseuille flow

If the shear Reynolds number, R_{eG} , is computed from Equ. (18) in the case Q = 25ml/min and for a 7.5 micron particle radius, one obtains G_{mean} = 1.23 s^{-1} and R_{eG} = 7.01 10^{-5}. This result has to be compared to the longitudinal (R_{ez}) or azimuthal Reynolds ($R_{e\omega}$) numbers presented in Table 1 showing that the lift effect on the particle in Part A of the device is a minor effect.

Consequently we do not consider it.

Longitudinal motion of the particle inside the esophagus

The longitudinal relative particle velocity , v_z (t) , is easily deduced from Equ. (16) since

$v_z(t) = \dot{z}$.

Equ. (16) becomes :

$$m_P \frac{dv_z(t)}{dt} = -k\, v_z(t) \qquad (29),$$

indicating that inertial effects are balanced by the frictional force exerted on the sphere by the fluid. The mathematical solution for such an equation involves an exponential term decreasing with time: exp(-kt/m_p). Since m_p = 1, 89 10^{-12} kg, and k (defined in Equ. (12) as $6\pi\, \eta_f\, a$) equals 1.41 10^{-7} Pa.s.m, the ratio k/m_p = 7.48 10^4 s^{-1}. The exp(-kt/m_p) term is thus essentially transient and will decay very quickly. It can be ignored and the absolute longitudinal velocity of the particle (in the laboratory frame) can be assumed to be roughly the same as the fluid velocity. This result is consistent with the fact that the particle radius is much smaller than the esophagus radius (a / R_1 = 7.5 10^{-6} m / 6 10^{-3} m ≈ 10^{-3}). The particle may be considered as a "tracer" and follows the fluid with the same speed as the local Poiseuille velocity [31]. The longitudinal position of the particle increases linearly with time:

$$z(r,t) = U_z(r)\, t \qquad (30).$$

A key point for tissue engineering applications is the residence time of a suspended cell in the bioreactor. Based on U_{mean} velocity, this residence time can be evaluated as: Δt =

esophagus length / U_{mean}. Since the esophagus length is roughly equal to 65 mm, for U_{mean} = 3,68 mm/s, a 17.7 s residence time is found.

Rotating motion of the particle

Multiplying Equ. (15) by the complex number i (i^2 = -1) and adding Equ. (14), this coupled system can be transformed in one equation in the complex domain as follows:

$$m_p \ddot{s} + \left(k + i\, 2 m_p \omega\right)\dot{s} - m_b \omega^2 s = -m_b\, g\, i\, e^{-i\omega t} \quad , \quad \text{where } s = x + iy \qquad (31).$$

This equation is consistent with the work of Kessler et al. [32].

Equ. (31) may be re-written as:

$$\ddot{s} + \left(\frac{k}{m_p} + 2\, i\, \omega\right)\dot{s} - \frac{m_b}{m_p}\omega^2 s = -\frac{m_b}{m_p}\, g\, i\, e^{-i\omega t} \qquad (32).$$

Solving Equ. (32) requires two steps:

* Solving the associated homogeneous equation:

$$\ddot{s} + \left(\frac{k}{m_p} + 2\, i\, \omega\right)\dot{s} - \frac{m_b}{m_p}\omega^2 s = 0 \qquad (33).$$

Convenient solutions for Equ. (33) , $s_h(t)$, are search as : $s_h(t) = \exp(\sigma t)$, with σ satisfying the condition:

$$\sigma^2 + \left(\frac{k}{m_p} + 2\, i\, \omega\right)\sigma - \frac{m_b}{m_p}\omega^2 = 0 \qquad (34).$$

Equ. (34) has two complex σ solutions that can be developed in leading orders of the small quantity ($\omega\, m_p / k$):

$$2\,\sigma_1 = -\left(\frac{k}{m_p} + 2i\omega\right) + \frac{k}{m_p}\left[1 + 2\frac{m_b}{m_p}\frac{m_p^2\omega^2}{k^2} + i\left(\frac{2\omega m_p}{k} - 4\frac{m_b}{m_p}\frac{\omega^3 m_p^3}{k^3}\right)\right] \qquad (35)$$

and

$$2\,\sigma_2 = -\left(\frac{k}{m_p} + 2i\omega\right) - \frac{k}{m_p}\left[1 + 2\frac{m_b}{m_p}\frac{m_p^2\,\omega^2}{k^2} + i\left(\frac{2\omega m_p}{k} - 4\frac{m_b}{m_p}\frac{\omega^3\, m_p^3}{k^3}\right)\right] \qquad (36).$$

Neglecting the term of order $\left(\frac{\omega^3 m_p^3}{k^3}\right)$ in Equ. (35) and (36), one obtains:

$$\sigma_1 \approx \frac{m_b\,\omega^2}{k} \qquad \text{and} \qquad \sigma_2 \approx -\frac{k}{m_p} - \frac{m_b\,\omega^2}{k} - 2\, i\, \omega \qquad (37).$$

This yields:

$$s_h(t) = C_1 e^{\frac{t}{\tau}} + C_2\, e^{-\frac{k}{mp}\, t}\, e^{-\frac{t}{\tau}}\, e^{-2i\omega t} \qquad (38),$$

where $\tau = k / m_b\, \omega^2$ has the physical meaning of a centrifugal time, and a numerical value of $5.9\ 10^5$ s (obtained with k = 1, 41 10^{-7} Pa.s.m, $\omega = 1.57\ s^{-1}$, $m_b = 9, 72\ 10^{-14}$ kg).

C_1 and C_2 are integration constants.

As previously explained the $\exp(-kt/m_p)$ term will decay very quickly. Consequently all the C_2 term can be ignored and $s_h(t)$ may be approximated as:

$$s_h(t) \approx C_1 e^{\frac{t}{\tau}} \approx C_1\, (1 + \frac{t}{\tau}) \qquad (39).$$

* Searching a particular solution, $s_p(t)$, of the complete equation in the form $\beta \exp(-i\omega t)$.

One easily obtains:

$$s_p(t) = \beta\, e^{-i\,\omega t} \quad with \quad \beta = \frac{m_b\, g}{\omega\, k \left[1 - \frac{(m_b - m_p)\, i\, \omega}{k}\right]} \qquad (40).$$

Observing that the term $\frac{m_b\, g}{k}$ is exactly the sedimentation velocity u_p defined in Equ. (27), and that the term $(m_b - m_p)\, \omega / k$ is of order 10^{-5}, the solution $s_p(t)$ can be reduced to:

$$s_p(t) = \frac{u_p}{\omega}\, (\cos(\omega t) - i \sin(\omega t)) \qquad (41).$$

Finally $s(t) = s_h(t) + s_p(t)$. The integration constant C_1 is determined by the initial condition: $s(0) = s_0 = C_1 + u_p / \omega$. So that:

$$s(t) = \left(s_0 - \frac{u_p}{\omega}\right) e^{\frac{t}{\tau}} + \frac{u_p}{\omega}\, e^{-i\omega t} \qquad (42).$$

Coming back to the real and imaginary part of $s(t) = x(t) + i\, y(t)$, the rotating trajectory of the particle is described by equations (43) and (44):

$$x(t) = \left(x_0 - \frac{u_p}{\omega}\right) e^{\frac{t}{\tau}} + \frac{u_p}{\omega} \cos(\omega t) \qquad (43).$$

$$y(t) = y_0\, e^{\frac{t}{\tau}} - \frac{u_p}{\omega} \sin(\omega t) \qquad (44).$$

We thus confirm the solution proposed by Kessler et al. [32].

It is interesting to note that the terms associated with Coriolis force may be directly neglected in Equ. (14-15), so that the equations to solve become decoupled:

$$m_P\,\ddot{x} + k\dot{x} - m_b\omega^2 x = -m_b\, g\, sin\,(\omega t) \quad (45)$$

$$m_P\,\ddot{y} + k\dot{y} - m_b\omega^2 y = -m_b\, g\, cos\,(\omega t) \quad (46).$$

Solving separately Equ. (45) and (46) leads to:

$$x(t) = \left(x_0 - \frac{u_p}{\omega}\right) e^{\frac{t}{\tau}} + \frac{u_p}{\omega}\cos(\omega t) + \frac{u_p}{\omega}\frac{(m_p + m_b)\omega}{k}\sin(\omega t) \quad (47).$$

$$y(t) = y_0\, e^{\frac{t}{\tau}} - \frac{u_p}{\omega}\sin(\omega t) + \frac{u_p}{\omega}\frac{(m_p + m_b)\omega}{k}\cos(\omega t) \quad (48).$$

The quantity $(m_p + m_b)\,\omega\,/k$ being of order 10^{-5}, the associated terms can be dropped and one finds again expression (43) as a solution for x(t) and expression (44) as a solution for y(t).

An illustration of the trajectory described by Equ. (43) and (44) is shown in **Figure 3**, with x_0 = 3000 µm, and y_0 = 100 µm as an initial position for the particle, u_p = 6.74 µm/s, τ = 5.9 10^5 s and ω = 15 r.p.m. = $\pi/2$ s^{-1} ($\approx$ 1.57 s^{-1}). The particle follows a periodic nearly circular path in the clockwise direction, associated with a very slow centrifugal drift towards the esophagus wall. Since $\omega = \pi/2$ s^{-1} , one turn is achieved each multiple of t = 4s. According to the estimation of its residence time in the esophagus (about 17.7s) the particle can execute only four complete turns before leaving the esophagus. The particle paths in the first turn and 4^{th} turn are represented in **Figure 3**.

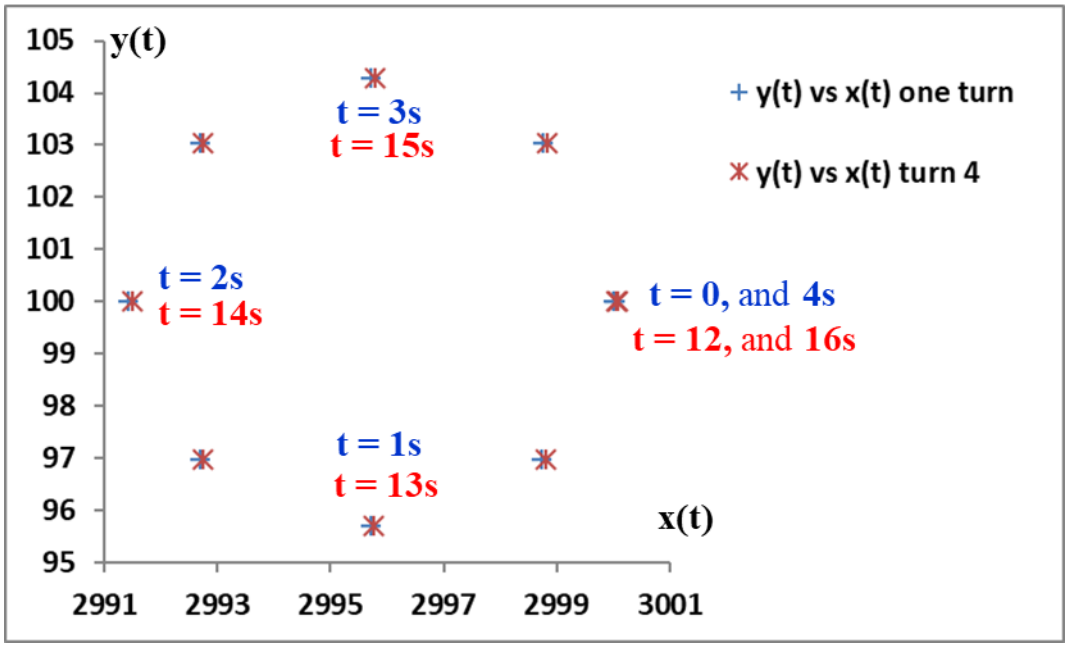

Figure 3 – Particle path in the rotating frame, as described by Equ. (43) and (44). The initial position for the particle is chosen as: x_0 = 3000 μm, and y_0 = 100 μm. Other numerical values are: u_p = 6.74 μm/s, τ = 5.9 10^5 s and ω = 15 r.p.m. Units for x(t) and y(t) are microns.

Inside the esophagus (**Part A**) this nearly circular motion is combined with the longitudinal motion described by Equ. (30). This generates spiral trajectories within the esophagus.

Equ. (43) and (44) show that the centrifugal drift of the particle is governed by the centrifugal time τ, and that the radius of the orbit is proportional to the sedimentation velocity u_p and inversely proportional to the rotation rate ω. The centrifugal shift is more and more negligible when τ increases. This may occur if the suspending medium viscosity η_f or the particle radius a increases. Conversely if the difference between the particle and suspending medium density increases or if ω increases, τ will decrease and the centrifugal shift will be more important. Increasing ω or η_f will also reduce the radius of the orbit whereas increasing the density difference (ρ_p -ρ_f) and the particle radius a will increase u_p, and thus the circular path radius. A synopsis of the influence of the governing physical quantities on the particle motion described by Equ. (43) and (44) is presented in **Table 2**.

Parameter increase	Effect on the viscous drag coefficient k	Effect on the sedimentation velocity u_p	Effect on the centrifugal time τ	Effect on the orbit radius (u_p/ω)
$\eta_f \uparrow$	Increase	Decrease	Increase	Decrease
$\omega \uparrow$	-----	----	Decrease	Decrease
$(\rho_p - \rho_f) \uparrow$	-----	Increase	Decrease	Increase
a $\uparrow$	Increase	Increase	Increase	Increase

Table 2. Influence of the main parameters of the problem on the quantities describing the particle motion.

The particle motion X(t) and Y(t) in the ground-based frame may be easily obtained from equ. (43) and (44):

$$X(t) = \frac{u_p}{\omega} + \left(x_0 - \frac{u_p}{\omega}\right) e^{\frac{t}{\tau}} \cos(\omega t) - y_0\, e^{\frac{t}{\tau}} \sin(\omega t) \quad (49).$$

$$Y(t) = \left(x_0 - \frac{u_p}{\omega}\right) e^{\frac{t}{\tau}} \sin(\omega t) + y_0\, e^{\frac{t}{\tau}} \cos(\omega t) \quad (50).$$

Since $$(X(t) - \frac{u_p}{\omega})^2 + Y^2(t) = \left[\left(x_0 - \frac{u_p}{\omega}\right)^2 + y_0^2\right] e^{\frac{2t}{\tau}} \quad (51),$$

one can recognize a circle with an increasing radius and a stationary center. The rotation along this circle is counter-clockwise. The physical parameters influencing the particle trajectory remain the quantity (u_p/ω) and the centrifugal time τ.

4 Discussion

The particles trajectories predicted by Equ. (43) and (44) as well as Equ. (49)-(51) are in excellent agreement with the experimental results of Pollack et al. [16] and Wolf and Schwarz [33]. Pollack et al. [16] observed that in the rotating frame of reference, microcarriers with density greater than the surrounding medium followed a circular motion relative to the culture medium combined with a migration towards the outer wall of the reactor. In the rotating frame, the direction of the gravitational force changes cyclically and

518 over a complete revolution of the chamber the particles experience an average gravitational
519 force about zero. Rotating bioreactors are thus said to simulate microgravity environment. In
520 their experiments polystyrene beads with a density of 1050 kg/m^3 and 0.5 mm diameter
521 radius were suspended in distilled water at 23°C. The bioreactor was rotated at 18 rpm. Their
522 results confirm that the microcarriers sedimentation velocity does not depend on ω, and is
523 the same as in free fall conditions.
524 Experiments by Wolf and Schwarz [33] examined parameters (gravitational strength, fluid
525 rotation rate, particle sedimentation rate, and particle initial position) within the useful range
526 for tissue cultures in NASA rotating wall culture bioreactors. They observed that the rotating
527 fluid effectively counters sedimentation. Biological tissue was simulated by nearly spherical
528 pieces of sponge suspended in water, with typical sizes of a few centimeters. The device
529 used was the NASA Slow Turning Lateral Vessel (STLV). Results from this group
530 demonstrate that the speed of the particle motion through the rotating fluid medium is the
531 same as its terminal sedimentation rate through a stationary fluid (for identical gravitational
532 conditions). They also demonstrate that the diameter of the nearly circular path is reduced
533 for the lower sedimentation rate and that it is increased for augmented gravitational
534 acceleration. They show that increasing the angular rotation rate from 8.64 r.pm. to 17.7
535 r.p.m. induces a reduction of the diameter of the particle path.
536 In tissue engineering applications, the size of the suspended particles may change during the
537 culture due to cell proliferation and/or recruitment of additional cells into an aggregate,
538 causing an increase in sedimentation velocity by the square of the radius. To counteract the
539 increase in sedimentation velocity the speed of rotation may be augmented.
540 However from an experimental point of view, a low shear environment has to be maintained
541 during cell cultivation (especially in recellularisation experiments). From a theoretical point
542 of view, the mathematical descriptions presented in this paper are valid when the spheres and
543 the rotation rate are sufficiently small so that viscosity dominates and the Reynolds numbers
544 remain small. As explained in Section 3.2.2, for a 25ml/min perfusion flow and for a 7.5

545 micron particle radius, a representative value of the shear rate is G_{mean} = 1.23 s^{-1},
546 corresponding to 1.23 mPa shear stress. For the sake of comparison values reported by
547 Grimm et al. [22] are of order 180-320 mPa for 50 μm spherical beads, and 500 mPa for 3D
548 aggregates of BHK-21 cells, in a Rotating Wall Vessel (RWV).

549 In order to minimize mechanical damage to cultured cells optimal setting of the peristaltic
550 pump is required: choice of the tubing, low pump motor speed, minimized occlusion by the
551 roller heads. Complete filling of the chamber and solid body rotation of the culture medium
552 should also be achieved. The fluid thus rotates at the same angular velocity as the chamber
553 walls and thereby creates a laminar flow with minimal shear force. Complete filling of both
554 **Part A** and **Part B** of our device also minimizes the influence of the deformability and
555 porosity of the esophagus wall, that are not taken into account in the present theoretical
556 analysis. However Varley et al. [19] experimentally captured the flow velocity vectors in a
557 RWV bioreactor for cell culture under different speeds of rotation and different filling rates
558 (60%, 85%, 100%) and they concluded that 85% fill volume is an optimum condition as
559 regards cell oxygenation and proliferation . The presence of both fluid and air within the
560 chamber could increase the surface area for gas exchange. These authors do not address the
561 question of pressure and air compressibility.

562 One important limitation of the present study remains the entry length in the esophagus (
563 given in **Table 1**). If Q = 25ml/min, the entry length represents 41% of the esophagus total
564 length thus limiting the validity of the theoretical analysis to the remaining 59%. The length
565 of the tissue construct is thus important in such type of devices: the longer it will be, the
566 lower will be the relative importance of entry and exit flow perturbations. A numerical study
567 of the flow inside the RCCSmax bioreactor would allow to describe more precisely the
568 esophagus entry and outlet area (possible flow stagnation or cell accumulation).

569 **5 Conclusion**

The RCCS Synthecon bioreactor appears to be a convenient device for cell culture and esophagus tissue engineering since it allows controlled mechanical stimulation, through the combination of flow perfusion and rotation. Cells or particles are constantly maintained in suspension in the media, which insures that nutrient, oxygen, and waste transfer will not be limited by diffusion as they are in static culture systems. Forces that might damage cells are minimized in this device and a low shear stress environment is created provided that the perfusion rate and the rotation speed remain moderate ($\omega < 20$ rpm and $Q < 30$ ml/min).

Acknowledgements: The authors would like to thank Madam Michelle Westaway for her careful checking of the english writing.

Competing interests: None declared.

Funding: Agence de Biomédecine; Inserm; Région Nouvelle-Aquitaine.

Ethical approval: Not required.

References

• [1] Zambon J.P., Atala A., and Yoo J. Methods to generate tissue-derived constructs for regenerative medicine applications. Methods. 2020; 171: 3-10. DOI: 10.1016/j.ymeth.2019.09.016

[2] Choudhury D., Yee M., Sheng Z., Amirul A. and Naing M. Decellularization systems and devices: state of the art. Acta Biomaterialia, Part A. 2020; 115: 51-59. https://doi.org/10.1016/j.actbio.2020.07.060

[3] Shaw-Smith C. Oesophageal atresia, tracheao-oesophageal fistula, and the VACTERL association: review of genetics and epidemiology. Jour. of Medical Genetics. 2006; 43 (7): 545-554. doi: 10.1136/jmg.2005.038158.

[4] Domper-Arnal M.J., Ferrandez Arenas A., and Lanas Arbeloa A. Esophageal cancer : risk factors, screening and endoscopic treatment in Western and Eastern countries . World Jour. of Gastroenterology. 2015; 21 (26): 7933-7943. doi: 10.3748/wjg.v21.i26.7933

[5] Sitthisang S., Leong M.F., and Chian K.S. Perfusion decellularization of porcine esophagus: Study of two processing factors affecting the folded mucosal structure of the esophageal scaffold. Journal of Biomedical Material Research, Part A. 2021; 109 (5):745-753. **https://doi.org/10.1002/jbm.a.37060**

[6] Arakelian L., Godefroy W., Faivre L. and Cattan P. Esophagus Decellularization. In: Kajbafzadeh AM (Eds) Decellularization Methods of Tissue and Whole Organ in Tissue Engineering. Advances in Experimental Medicine and Biology. 2021; 1345: 7-15. Springer, Cham. DOI: 10.1007/978-3-030-82735-9_2

[7] Nayakawde N.B., Methe K., Banerjee D., Berg M., Premaratne G.U., and Olausson M. In Vitro Regeneration of Decellularized Pig Esophagus Using Human Amniotic Stem Cells. BioResearch Open Access. 2020; 9(1): 22–36. https://doi.org/10.1089/biores.2019.0054

[8] Arakelian L., Caille C., Faivre L., Corté L., Bruneval P., Shamdani S. et al. A clinical-grade acellular matrix for esophageal replacement. Journal of Tissue Engineering and Regenerative Medicine. 2019; 13(12) : 2191-2203. DOI: 10.1002/term.2983

[9] Luc G., Charles G., Gronnier C., Cabau M., Kalisky Ch., Meulle M. et al. Decellularized and matured esophageal scaffold for circumferential esophagus replacement: proof of concept in a pig model. Biomaterials. 2018; 175: p1-18. https://doi.org/10.1016/j.biomaterials.2018.05.023

[10] https://synthecon.com/pages/perfusion_bioreactor_system_rccmax_dual_synthecon_40.asp

[11] Dedolph R., and Dipert M. The physical basis of gravity stimulus nullification by clinostat rotation. The Plant Physiology. 1971; 47:756-764. doi: 10.1104/pp.47.6.756

[12] Freed L., Pellis N., Searby N., de Luis J., Preda C., Bordonaro J., and Vunjak-Novakovic G. Microgravity cultivation of cells and tissues. Gravitational and Space Biology Bulletin. 1999; 12(2) : 57-66.

[13] Klaus D. Clinostats and bioreactors. Gravitational and Space Biology Bulletin. 2001; 14(2): 55-64.

[14] Hammond T. and Hammond J. Optimized suspension culture: the rotating – wall vessel. Am. Jour. Physiol. Renal Physiol. 2001; 281: F12-F25. doi: 10.1152/ajprenal.2001.281.1.F12.

[15] Ramdan M., and Sukmana I. Advanced bioreactor system for the implantable biomaterials testing and tissue engineering applications. ARPN Jour. of Engineering and Applied Sciences. 2017; 12 (12) : 3767-3771.

[16] Pollack S., Meaney D., Levine E., Litt M., and Johnston E. Numerical model and experimental validation of microcarrier motion in a rotating bioreactor. Tissue Engineering. 2000; 6 (5) : 519-530. DOI: 10.1089/107632700750022161

[17] Mazzoleni G., Boukhechba F., Steimberg N., Boniotti J., Bouler J.M. and Rochet N. Impact of dynamic culture in the RCCS bioreactor on a three-dimensional model of bone matrix formation. Procedia Engineering. 2011; 10 : 3662-3667. doi:10.1016/j.proeng.2011.04.603

[18] Ferrarini M., Steimberg N., Ponzoni M., Belloni D., Berenzi A., Girlanda S., et al. Ex-vivo dynamic 3D culture of human tissues in the RCCS™ bioreactor allows the study of

multiple myeloma biology and response to therapy. PLOSone. 2013;8(8): e71613. https://doi.org/10.1371/journal.pone.0071613

[19] Varley M., Markaki A. and Brooks R. Effect of rotation on scaffold motion and cell growth in rotating bioreactors. Tissue Engineering, Part A. 2017; 23 (11 and 12) : 522-534. doi: 10.1089/ten.tea.2016.0357

[20] Liu T., Li X., Sun X., Ma X. and Cui Z. Analysis on forces and movement of cultivated particles in a rotating wall vessel bioreactor. Biochemical Engineering Journal. 2004; 18: 97-104. https://doi.org/10.1016/S1369-703X(03)00171-2

[21] Begley C., Kleis S. The fluid dynamic and shear environment in the NASA/JSC rotating-wall perfused-vessel bioreactor. Biotechnology BioEngineering. 2000; 70(1) : 32-40. DOI: 10.1002/1097-0290(20001005)70:1<32::aid-bit5>3.0.co;2-v

[22] Grimm D., Wehland M. , Pietsch J., Aleshcheva G., Wise P., Van Loon J. et al. Growing tissues in real and simulated microgravity: new methods for tissue engineering. Tissue Engineering, Part B. 2014; 20 (6) : 555- 566. DOI: 10.1089/ten.TEB.2013.0704

[23] Burova I., Wall I., and Shipley R. Mathematical and computational models for bone tissue engineering in bioreactor systems. Journal of Tissue Engineering, 2019; 10 : 1-25. doi: 10.1177/2041731419827922

[24] Morabito C., Steimberg N., Mazzoleni G., Guarnieri S., Fano-Illic G. and Mariggio M. RCCS bioreactor-based modelled microgravity induces significant changes on in vitro 3D neuroglial cell cultures. Bio Med Research International . 2015; article ID754283. https://doi.org/10.1155/2015/754283

[25] Lei X., Ning L, Cao Y., Liu S., Zhang S., Qiu Z. et al. NASA-approved rotary bioreactor enhances proliferation of human epidermal stem cells and supports formation of 3D epidermis-like structure. PLOSone. 2011; 6 (11) : e26603. https://doi.org/10.1371/journal.pone.0026603

[26] Asnaghi A., Jungebluth P., Raimondi M., Dickinson S., Rees L., Go T. et al. A double-chamber rotating bioreactor for the development of tissue-engineered hollow organs: from concept to clinical trial. Biomaterials, 2009; 30 : 5260-5269. DOI: 10.1016/j.biomaterials.2009.07.018

[27] Lee H., Marin-Araujo A., Aoki F., Haykal S., Waddell T., Amon C. et al. Computational fluid dynamics for enhanced tracheal bioreactor design and long-segment graft recellularization. Nature - Scientific Reports, 2021; 11:1187. https://doi.org/10.1038/s41598-020-80841-w

[28] Urbani L., Camilli C., Phylactopoulos D., Crowley C., Natarajan D., Scottoni F. et al. Multi-stage bioengineering of a layered oesophagus with in vitro expanded muscle and epithelial adult progenitors. Nature Communications. 2018; 9: 4286. https://doi.org/10.1038/s41467-018-06385-w

[29] Pier B. and Govindarajan R. Nonlinear travelling waves in rotating Hagen-Poiseuille flow. Fluid Dynamics Research. 2018; 50 (3): 031402. DOI :10.1088/1873-7005/aaaa9f

[30] Matas J.P., Morris J. and Guazzelli E. Inertial migration of rigid spherical particles in Poiseuille flow . Jour. Fluid Mech. 2003; 515 :171-195. DOI: https://doi.org/10.1017/S0022112004000254

[31] Bhattacharya S., Misrah C. and Bhattacharya S. Analysis of general creeping motion of a sphere inside a cylinder. Jour. Fluid Mech., 2010; 642: 295-328. DOI: https://doi.org/10.1017/S0022112009991789

[32] Kessler J. , Hill N. , Strittmatter R. and Wiseley D. Sedimenting particles and swimming micro-organisms in a rotating fluid. Adv. Space Res. 1998; 21 (8/9) : 1269-1275. https://doi.org/10.1016/S0273-1177(97)00398-0

[33] Wolf D. and Schwarz R. Experimental Measurement of the orbital paths of particles sedimenting within a rotating viscous fluid as influenced by gravity. NASA Technical Paper 3200. 1992.